IMAGING ELECTRICAL CURRENT DENSITY USING 0.15T MAGNETIC RESONANCE IMAGING SYSTEM

O. Özbek[1], Ö. Birgül[1], B. M. Eyüboglu[1], Y. Z. Ider[2]
[1]Middle East Technical University, Dept. of Electrical and Electronics Engineering, Ankara, Turkey
[2] Bilkent University, Dept. of Electrical and Electronics Engineering, Ankara, Turkey

Abstract- **In this study, imaging of electrical current density in conducting objects, which contain nuclear magnetic resonance (NMR) active nuclei is planned using 0.15T Magnetic Resonance Imaging (MRI) system. Current to be imaged is externally applied to the object in synchrony with a standard spin-echo pulse sequence. Applied current is a bipolar DC current pulse, which creates a DC current density at each cycle within the object. The applied current pulse creates a measurable magnetic flux density. The component of magnetic flux density parallel to the main magnetic field accumulates an additional phase in the phase of the complex MR image. Magnetic flux density can be extracted using two phase images acquired with and without the current pulse. Measurement of all three components of magnetic flux density makes the reconstruction of current density possible with a spatial resolution equal to the half of the MR resolution. Experiments performed on several phantoms and the results are presented.**

Keywords **- Magnetic Resonance Imaging, Current Density Imaging**

I. INTRODUCTION

Knowledge of spatial distribution of externally applied electrical current to the body provides vital information in many applications of biomedical engineering. For example, current density distribution on the myocardium during cardiac defibrillation is very important to optimize the defibrillation efficacy [1, 2, 3]. Determination of electrical current density applied between a pair of electrodes can be used to determine lead-sensitivity maps of biopotential recording set-ups [4]. Finally, accurate measurement of current density distribution may lead to high fidelity conductivity imaging [5].

Nuclear magnetic resonance imaging techniques can be used to image the current density $\vec{J}$. Joy *et al.* [6] and Scott *et al.* [7, 8] have demonstrated the possibility of imaging current density inside a volume conductor, which contains Nuclear Magnetic Resonance (NMR) active nuclei, by using MRI. Referred studies have been carried on a 2T MRI System. In this work, a 0.15T Imaging System is used. Current, which is planned to be imaged, is externally applied to the object by a bipolar current source in synchrony with a standard spin-echo pulse sequence. The applied current pulse creates a magnetic flux density within the object. The parallel component of magnetic flux density to the main magnetic field causes an additional phase accumulation in the phase of the complex MR image. This accumulated magnetic flux density is extracted using two phase images acquired with and without current pulse.

II. THEORY

To obtain the current density, ratio of the two complex images of the object, with and without the current pulse, is taken. This difference will be proportional to the magnetic flux density due to the applied current. Then, using Ampere's law, current density can be obtained from the magnetic flux density. The acquired NMR signal using a spin echo pulse sequence can be expressed as [9],

$$S(k_x, k_y, t) = \int_x \int_y M(x,y) \exp\{j[\gamma B t + \phi_c + k_x x + k_y y]\}\, dx\, dy \quad (1)$$

Here, $M(x,y)$ is the real transverse magnetization, B is the inhomogeneity component of the magnetic flux density, ϕ_c is a constant phase due to the instrumentation. $k_x=\gamma G_x t$ and $k_y=\gamma G_y t_y$, where G_x and G_y are frequency encoding and phase encoding gradient strengths respectively. γ is the gyromagnetic constant, t_y is the duration of the phase encoding gradient, and t is the data acquisition time.

The applied DC current pulse creates a constant magnetic field. The parallel component of this magnetic field with the main magnetic field accumulates an additional phase term in the signal equation. Then, the signal equation (1) becomes

$$S(k_x, k_y, t) = \int_x \int_y M(x,y) \exp\{j[\gamma B t + \phi_c + \gamma B_j(x,y) T_c + (k_x x + k_y y)]\}\, dx\, dy \quad (2)$$

where, B_j is the parallel component of the current induced magnetic field with the main magnetic field, and T_c is the total duration of applied current. Taking the Fourier transform of $S(k_x,k_y,t)$ with respect to k_x and k_y, magnetization density can be reconstructed. The obtained magnetization densities for both with and without current flow cases are,

$$M_c(x,y) = M(x,y) \exp[j\gamma B t + j\phi_c] \quad (3)$$

and

$$M_{cj}(x,y) = M(x,y) \exp\{j\gamma[Bt + B_j(x,y) T_c] + j\phi_c\} \quad (4)$$

respectively. Taking the ratio of (4) to (3),

$$\frac{M_{cj}(x,y)}{M_c(x,y)} = \frac{M(x,y) \exp\{j\gamma[Bt + B_j(x,y)T_c] + j\phi_c\}}{M(x,y)\exp[j\gamma B t + j\phi_c]} = \exp[j\gamma B_j(x,y) T_c] \quad (5)$$

Here, $\gamma B_j(x,y) T_c$ is the normalized phase term. Simply scaling the phase term with γT_c, magnetic flux density due to the applied current can be obtained. Finally, by using Ampere's law (6), current density can be calculated.

$$\vec{J} = \frac{(\nabla \times \vec{B})}{\mu_0} \tag{6}$$

Here $\nabla\times$ represents the curl operation and μ_0 is the permeability of free space.

III. Methodology

As described in (6), $\vec{J}$ can be obtained by using three components of B. Since only the parallel component of B with the main magnetic field is measurable in one configuration, three sets of measurements as shown in Fig. 1, will be taken.

The phantom used in this work is a 15x15x2cm rectangular prism shaped phantom, which is described in the following section. The third dimension of the phantom is so small compared with the other two dimensions that the current can be assumed to flow only in 2D (x-y plane). So, J_z will be zero.

In order to measure B_z, the phantom is placed in the magnet such that its z-axis is parallel with B_0 (Fig. 1a). Two axial images of the object, with and without a current pulse, are acquired. The derivative of normalized phase image, B_z, with respect to x and y are calculated. To obtain $\partial B_y/\partial z$, the phantom must be placed as in Fig. 1b. Assuming that the phantom is standing at $z=0$, sagittal images of slices at $z= -\Delta z$ and $z= \Delta z$ must be obtained. The difference of two phase images gives the desired differential term. Finally, $\partial B_x/\partial z$ is found repeating the same procedure as in the case of $\partial B_y/\partial z$ with different phantom orientation (Fig. 1c).

IV. Experimental Setup

A. Hardware

In this work, a resistive air core Oxford 0.15T magnet with 80cm bore generates the main magnetic field of the MRI system. The RF coil used is a saddle coil with 30cm diameter and 3 turns on either side. It is tuned to 6.4 MHz. Data acquisition hardware is composed of a PC and home made data acquisition electronics.

B. Phantom

A 15x15x2cm rectangular prism phantom is used. The phantom is shown in Fig. 1, schematically. The phantom is filled with 12.5g/l NaCl, 2g/l $CuSO_4 \bullet H_2O$ solution. 2x1cm rectangular copper electrodes with 1mm thickness are attached to both sides of the phantom. The phantom is fixed inside the RF coil by using a styro-foam mold.

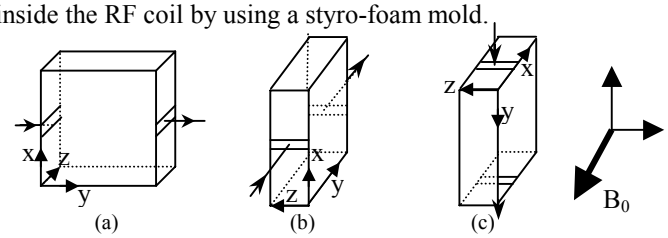

Fig. 1. Three phantom orientation, used during data collection

In order to keep the current carrying wires parallel to each other and at fixed positions during data acquisition, they are attached to the RF coil.

C. Pulse Sequence

A standard spin echo pulse sequence with and without bipolar current pulses is used. The pulse sequence is given in Fig. 2. The pulse repetition time (T_R) is 250ms, the echo time (T_E) is 58.4ms, and the amplitude of the injected current is 21mA. Total current injection time, T_C, is 40ms. A DSP card (Texas Instruments TMS320C25) installed in the PC generates both the pulse sequence and the current pulses. By doing so, the DC current pulse is synchronized with the pulse sequence. Due to the current pulse applied after the 90° RF pulse, an additional phase accumulates in the spins. If the same current pulse is applied after the 180° pulse, the added phase will dephase, therefore the polarity of the current pulse applied after 180° pulse is toggled.

D. Current Source

A voltage-controlled DC current source is designed and implemented. The voltage source is synchronized with the pulse sequence using two digital signals from the DSP card. In order to avoid RF interference, the current source is located in the Faraday cage and is operated by a battery supply. The digital inputs are coupled to the system optically through the Faraday cage.

V. Results

As described in the previous sections, two sets of complex MR images of the phantom are acquired, with and without current pulse. The normalized phase image is obtained by taking the ratio of the first phase image to the second one. Examples of magnitude and phase images and normalized phase image are shown in Fig. 3a-3e. These images are axial and they are acquired when the phantom is positioned as in Fig. 1a. Injected current density acts like a local gradient, and adds a phase to the MR signal. Change in the phase with the application of current can be observed when Fig. 3c. and Fig. 3d. are compared.

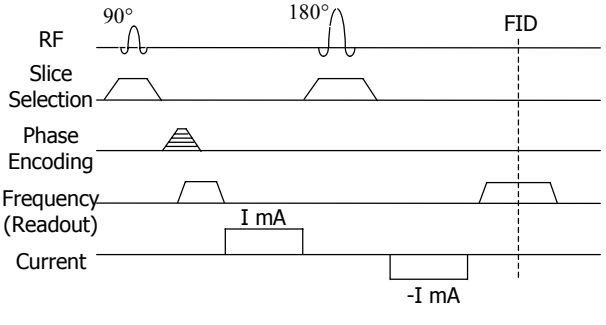

Fig. 2. Pulse sequence used in MRCDI

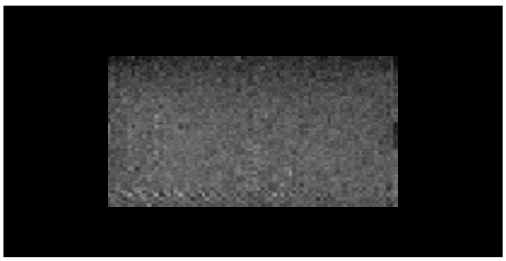

Fig. 3a. Magnitude image without current pulse

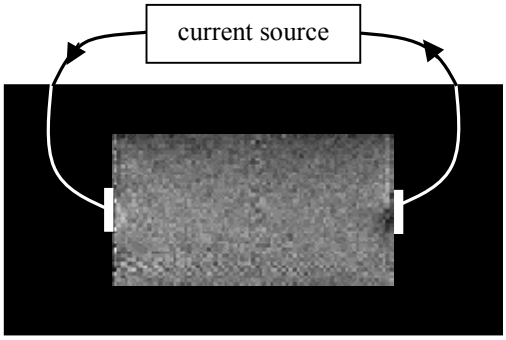

Fig. 3b. Magnitude image with current pulse

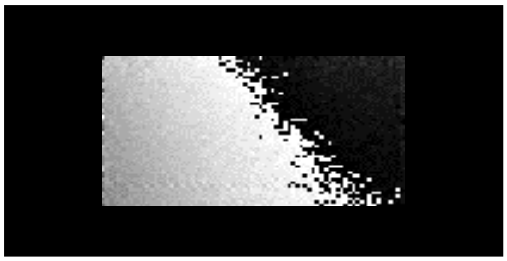

Fig. 3c. Phase image without current pulse

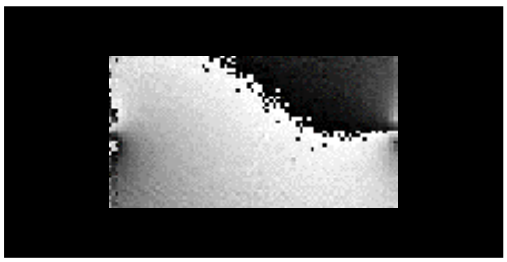

Fig. 3d. Phase image with current pulse

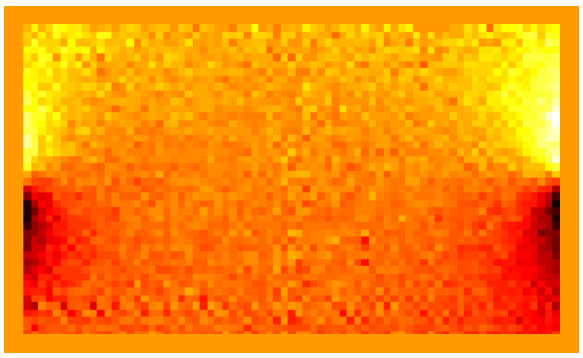

Fig. 3e. Phase unwrapped normalized phase image.

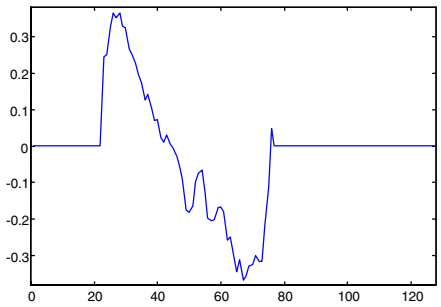

Fig. 3f. A profile of magnetic flux density through the midpoint between the two electrodes

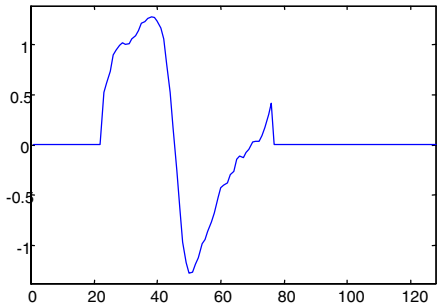

Fig. 3g. A profile of magnetic flux density through the current injecting electrode

The two phase images are utilized to obtain the normalized phase image (Fig. 3e) which is in fact a scaled version of the *B* field. As observed in Fig. 3c and 3d, there may be phase wraps in the phase images. Before calculating the flux density, these phase wraps need to be removed. To achieve this, a model-based phase unwrapping algorithm described by Liang [10] is used. In this configuration, *z*-axis of the phantom is parallel with B_0, so the normalized phase image is the scaled version of B_z component of *B* field. Current injection and current sink electrodes are on the left and on the right in the figure, respectively. In this image, darker regions represent the magnetic flux density pointing into the page, while lighter ones represent the magnetic flux density out of the page.

Regions close to the electrodes in Fig. 3e have higher contrast in the image. This shows that the B field strength is greater at the edges of the electrodes, which implies that the current density is greater at these areas as expected. Two profiles of magnetic field along the *x*-axis of the phantom, -one through the current injecting electrode, and the other through the midpoint between the two electrodes- are given in Fig. 3f and Fig. 3g, respectively. The peak values of *B* in these two figures verify that *B* field strength, -so that the current density- is greater at the edges of the electrodes.

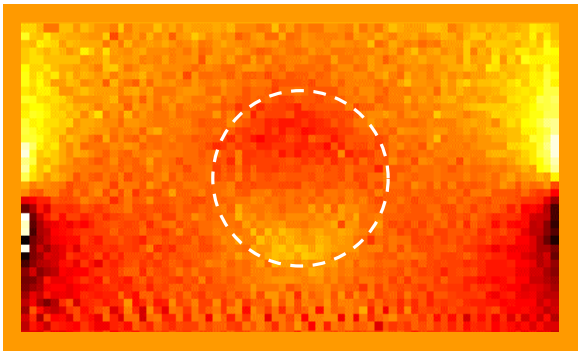

Fig. 4a. Phase unwrapped normalized phase image with a circular insulator at the center.

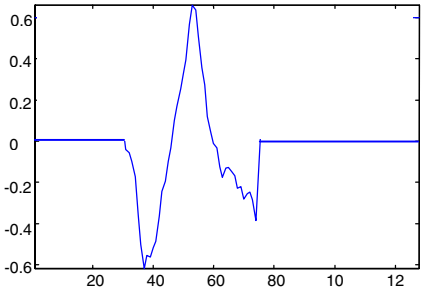

Fig. 4b. A profile of magnetic flux density through the mid-point between the two electrodes with a circular insulator at the center of the phantom.

A circular plastic object with 3.1 cm diameter is placed at the center of the phantom. No current flows inside the object since it is an insulator. The magnetic field generated by the current flowing around the object, and the *B*-field profile through the midpoint between the two electrodes, along the *x*-axis are given in Fig. 4a and Fig. 4b, respectively. There exists a non-uniform *B*-field distribution within the boundary of the object

VI. Conclusion

In this study, imaging of electrical current density in conducing objects is planned. For this, a bipolar DC current pulse is applied to the object in synchrony with a standard spin-echo pulse sequence.

To obtain the current density in one direction, two orthogonal components of magnetic flux density, which are orthogonal to the direction of current flow, are needed. In this imaging technique, only the magnetic flux density component parallel to the main magnetic field is measurable. Therefore, the object has to be rotated in each set of measurements such that B_j (B-field component to be measured) is aligned with B_0. This is the main limitation of this technique in applying to human subjects. To overcome the rotation problem, Scott *et al.* [11] implemented a new technique. In this technique, current density at Larmor frequency and parallel to the direction of B_0 can be imaged without rotating the sample to be imaged.

In this work, only B_z is measured so far. The measurements are taken using the configuration in Fig.1a. Two sets of measurements will be done as shown in Fig. 1b-c to obtain current density.

Current density imaging may provide vital information for many applications in biomedical engineering. Using the current density distribution on the myocardium during cardiac defibrillation, the cardiac efficacy may be optimized, or lead sensitivity maps of biopotential recordings can be determined. Finally, accurate measurement of current density distribution may lead to high fidelity conductivity imaging. A study aiming at reconstructing conductivity images using the current density measurement will also be presented at this conference [12].

Acknowledgment

This work is supported by Turkish Scientific and Technical Research Council (TÜBITAK) Research Grant EEEAG-198006. Authors would like to thank Mr. Emre Arpinar for his efforts in data collection.

References

[1] R.E. Ideker, P.D. Wolf, C. Alferness, W. Karassowska, and W.M. Smith "Current concepts for selecting the location, size and shape of defibrillation electrodes," *PACE* vol. 14. pp. 227-240, 1991.

[2] P. Kneppo and L. I. Titomir "Topographic concepts in computerized electrocardiology," *Critical Reviews in Biomedical Engineering,* vol. 19, no.5, pp. 343-418, 1992.

[3] R. A. Province, M. G. Fishler, and N. V. Thakor "Effects of defibrillation shock energy and timing on 3-D computer model of heart," *Annals of Biomedical Engineering* vol. 21, pp. 19-31, 1993.

[4] D. B. Geselowitz "An application of electrocardiographic lead theory to impedance plethysmography," *IEEE Transactions on Biomedical Engineering* vol. 18, pp. 18-38, 1971.

[5] J. G. Webster (Ed) *Electrical Impedance Tomography* pp. 224, 1990

[6] M. Joy, G. C. Scott, and R. M. Henkelman "In vivo detection of applied electric currents by magnetic resonance imaging," *Magnetic Resonance Imaging* vol. 7, pp. 89-94, 1989

[7] G. C. Scott, M. L. G. Joy, R. L. Armstrong, and R. M. Henkelman "Measurement of non-uniform current density by magnetic resonance," *IEEE Transactions on Medical Imaging* vol. 10, no. 3, pp. 362-374, 1991.

[8] G. C. Scott, M. L. G. Joy, R. L. Armstrong, and R. M. Henkelman "Sensitivity of magnetic resonance current-density imaging," *Journal of Magnetic Resonance* vol.97, pp.235-254, 1992.

[9] P. Mansfield and P. G. Morris *NMR Imaging in Biomedicine* pp. 32-80.

[10] Z. P. Liang "A model-based method for phase unwrapping," *IEEE Transactions on Medical Imaging* vol.15, no.6, pp.893-897, 1996

[11] G. C. Scott, M. L. G. Joy, R. L. Armstrong, and R. M. Henkelman, "Rotating frame RF current-density imaging," *Magnetic Resonance in Medicine* vol. 33, pp. 355-369, 1995.

[12] O. Birgul, O. Ozbek, B. M. Eyuboglu, and Y. Z. Ider, "Magnetic resonance-conductivity imaging using 0.15Tesla MRI scanner," *submitted to IEEE EMBS 23rd Annual Conference*